Degradation location study of proton exchange membrane at open circuit operation

Shaohua Xiao [a,b], Huamin Zhang [a,*], Cheng Bi [a,b], Yu Zhang [a], Yining Zhang [a,b], Hua Dai [a,b], Zhensheng Mai [a,b], Xianfeng Li [a]

[a] Lab of PEMFC Key Materials and Technologies, Dalian Institute of Chemical Physics, Chinese Academy of Sciences, Dalian 116023, China
[b] Graduate University of the Chinese Academy of Sciences, Beijing 100039, China

ABSTRACT

In order to investigate the location of the radical-initiated membrane degradation at open circuit operation, ceria (CeO_2) nanoparticles are firstly placed at different locations of the membranes to scavenge free radicals generated there. Scanning electron microscopy (SEM) is used to characterize cross-sectional morphology of membrane before and after the open circuit voltage (OCV) test. OCV decay rate is used as an indicator of membrane degradation rate. Composite membranes with CeO_2 nanoparticles facing anode or cathode show improved membrane durability than that of plain membrane in terms of OCV decay rate and cross-sectional morphology. CeO_2–Nafion composite membrane with the same thickness is subsequently proposed and it obtains the best durability. It is concluded that the chemical degradation at open circuit operation occurs at both sides of anode and cathode.

© 2010 Elsevier B.V. All rights reserved.

1. Introduction

Proton exchange membrane fuel cells (PEMFCs) are able to convert chemical energy directly into electrical energy electrochemically with high efficiency and low emission of pollutants, and have received much attention and great interest in the past decades [1,2]. Durability is one of the most necessary characteristics for PEMFCs to be accepted as a viable product. For example, the minimum lifetime of PEMFC for stationary applications is about 40,000 h, and around 20,000 h for transportation applications (buses) [3]. Membrane degradation has been proposed to be one of the crucial factors limiting the overall durability of PEMFCs [4]. As we know, proton exchange membrane (PEM) is to provide a conductive path, while at the same time separating the reactant gases and serving as an electronic insulator [5]. Perfluorosulfonic acid membranes such as Nafion® are widely used as the electrolyte membrane of PEMFCs because of its high conductivity as well as chemical and thermal stability [6]. However, membrane degradation was often detected in PEMFCs operation tests [7,8]. Membrane durability has been one of the primary obstacles for the commercialization of PEMFCs [9,10].

The evaluation of membrane durability under normal operating conditions is not practical because of its time consuming nature [11]. An alternative is to evaluate the fuel cell under accelerated lifetime tests [12,13]. It is widely accepted that open circuit voltage (OCV) test at low relative humidity (RH) with H_2 and O_2 as the reactant gases accelerates the membrane degradation and can be used as an effective test for evaluating membrane durability [14]. However, the mechanism at OCV accelerated test is not clear [9,10].

Free radicals (HO• and HOO•) are usually thought to be responsible for membrane degradation [15,16]. Two mechanisms regarding the location of the radical-initiated membrane degradation have been suggested [11,17,18]. The radicals could be generated at anode or cathode: (1) the direct formation during oxygen reduction reaction (ORR) via a two-electron pathway or the chemical combination of crossover hydrogen and oxygen at the cathode [7,12,19]; (2) a decomposition of H_2O_2 formed at the anode as a result of oxygen crossing from cathode to anode [20,21]. The hydrogen peroxide reacts with trace transition metals ions (found in membrane and/or catalysts) to form radicals [22]. Since there are no net electrochemical reactions taking place at the anode and cathode under open circuit operation, so the radicals cannot be obtained electrochemically. Additionally, H_2 or O_2 alone cannot damage the membrane even in the presence of the catalyst [23], and the membrane degradation can only happen in the case of the coexistence of H_2, O_2 and catalyst [24]. Therefore, the radicals are generated either through the chemical combination of crossover hydrogen and oxygen at the cathode or permeating O_2 and H_2 at anode, or at both sides of anode and cathode. The accelerated degradation at OCV test is generally attributed to the radicals generated by crossover gas [25]. However, the details of degradation at OCV test are still ambiguous. An example is the location of chemical degradation.
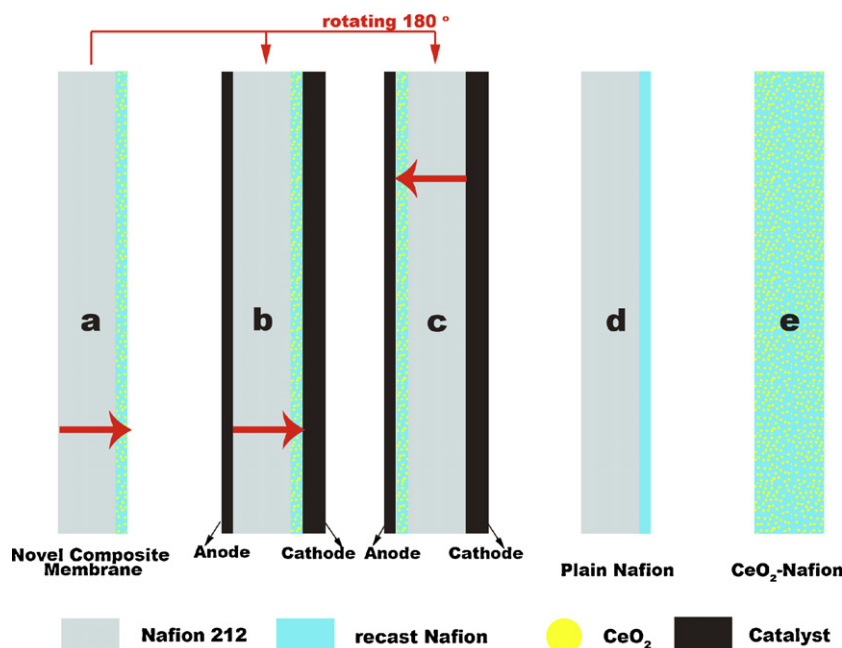
Fig. 1. Schematic diagrams of three kinds of composite membranes and two types of novel MEAs employing the novel composite membrane. (a) The novel composite membrane: Nafion® 212 combined with sprayed Nafion® layer with uniformly dispersed CeO$_2$ nanoparticles, (b) MEA-C, (c) MEA-A, (d) plain Nafion® (Nafion® 212 combined with sprayed Nafion® without CeO$_2$ nanoparticles), and (e) CeO$_2$–Nafion membrane. All the membranes are 60 μm.

Given the conflicting views on the degradation location, single-side-catalyzed membrane electrolyte assemblies (MEAs) without potential control were meant to simulate OCV test [22,26], providing access to separate the membrane degradation process into cathode and anode aspects. Clearly, this method deviated from regular fuel cell configuration. It also failed to reflect really electrochemical stressing at actual OCV test. From this point of view, it is very important to find a way for interpretation of degradation at OCV test.

It was reported that ceria (CeO$_2$) nanoparticles can effectively enhance membrane durability due to the faster reversible redox reaction (Ce$^{3+} \leftrightarrow$ Ce^{4+} + e$^-$) [27]. Babu et al. [28] pointed out that CeO$_2$ exhibited great promise to be used as a radical scavenger through electron paramagnetic resonance (EPR) spectroscopy. Trogadas et al. [29] reported that the loading and provenance (commercially obtained or synthesized in-house) of the ceria did not influence the fluorine emission rates (FER) at OCV test. Cs$_x$H$_{3-x}$PW$_{12}$O$_{40}$/CeO$_2$ was prepared to mitigate the membrane degradation and enhance cell performance simultaneously by Zhao et al. [30]. That is, CeO$_2$ nanoparticles can really scavenge free radicals occurred during the test, further increase the membrane durability, such as low OCV decay rate or low FER rate. CeO$_2$ nanoparticles can be employed to ascertain the free radical in terms of OCV decay rate indirectly.

This study is aimed at illuminating where the chemical degradation takes place at OCV test by means of varied locations of free radical scavenger CeO$_2$ nanoparticles in membranes. A novel composite membrane (Fig. 1a), using CeO$_2$ nanoparticles to ascertain the free radical, was first proposed to investigate the membrane degradation at anode and cathode. The novel composite membrane is composed of Nafion® 212 and a sprayed Nafion layer with uniformly dispersed CeO$_2$ nanoparticles, which can suppress free radicals. This unique design is able to separate the membrane degradation processes into anode side and cathode side, respectively at in situ OCV test. In this study, Nafion® resin is used as a model polymer material, and OCV decay rate is used as an indicator of the membrane degradation. The degradation at OCV test is investigated in detail here.

2. Experimental

2.1. Preparation of the novel composite membrane

As shown in Fig. 1a, the novel composite membrane is composed of Nafion® 212 combined with sprayed Nafion® layer with uniformly dispersed CeO$_2$ nanoparticles. The preparation procedure was as follows: firstly, CeO$_2$ nanoparticles (20 nm, Yuelong, China) were uniformly dispersed in the 5 wt% Nafion® (Du Pont, USA) isopropanol solution by ultrasonic bath. The mass ratio of Nafion® resin to CeO$_2$ was 6:1. Secondly, a piece of Nafion® 212 was extended over a flat glass plate and the resulting mixture was sprayed onto the upside of Nafion® 212, resulting in a layer of sprayed Nafion® at one side of the membrane. The thickness of the sprayed Nafion® layer was handled by controlling the amount of Nafion® solution. Finally, the composite membrane was dried at room temperature for 12 h. The thickness of the novel composite membrane was about 60 μm. For comparison, a plain Nafion® membrane (Fig. 1d) with the same thickness was prepared according to the same procedure.
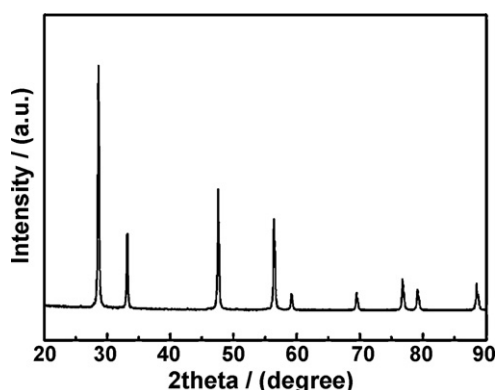

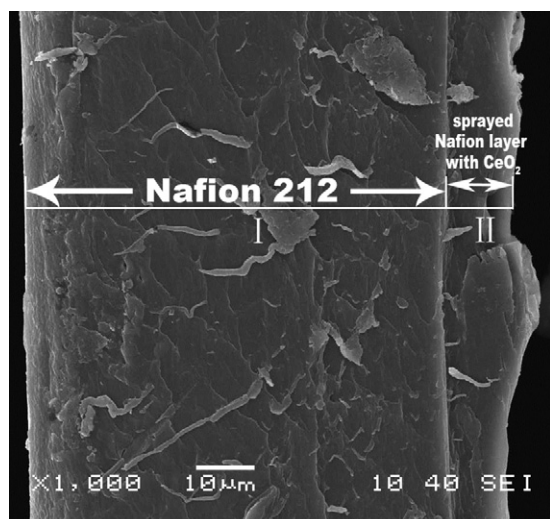**Fig. 2.** XRD spectrum of commercially obtained CeO$_2$ nanoparticles.

Fig. 3. SEM image of the cross-sectional morphology of the novel composite membrane.

CeO$_2$–Nafion composite membrane (Fig. 1e) was prepared by solution-casting method according to the following procedure [31,32]: Nafion® resin was obtained from 5 wt% Nafion®. The Nafion®/DMF solution and CeO$_2$ nanoparticles were mixed by ultrasonic bath to form an ink. Then the ink was poured onto a flat glass plate. The glass plate was first dried on a hot plate at 60 °C for 24 h then in a vacuum oven at 160 °C for 2 h. The amount of CeO$_2$ nanoparticles in the membrane was kept at 3 wt%. The thickness of the composite membranes was about 60 μm. This composite membrane was denoted as CeO$_2$–Nafion.

All membranes were retained at the same thickness because the membrane thickness made a difference on the membrane degradation according to Ghassemzadeh et al. [33]. Re-acidification of the membranes was carried out using 0.5 M H$_2$SO$_4$ solution for 1 h at 80 °C followed by de-ionized water treatment for 1 h at 80 °C.

2.2. Membrane electrode assembly (MEA) preparation and single cell evaluation

Two types of novel MEAs were obtained just by simply rotating the same novel membrane 180° (Fig. 1b and c). The control samples employing the plain Nafion® membrane (Fig. 1d) and CeO$_2$–Nafion membrane (Fig. 1e) were also fabricated, and the resulting MEAs were denoted as MEA-N and MEA-CeO$_2$, respectively. Therefore, four different MEAs were fabricated, they were as follows:
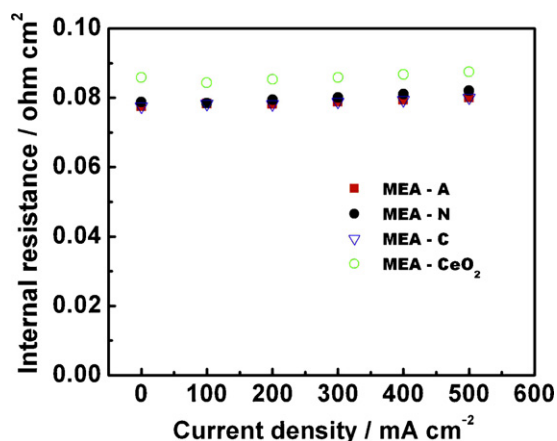

Fig. 4. Performance comparison of single cell employing different MEAs with fully humidified H$_2$/O$_2$ at 80 °C and 0.2 MPa.

Fig. 5. Internal resistance comparison of single cell employing different MEAs with fully humidified H$_2$/O$_2$ at 80 °C and 0.2 MPa.

(1) MEA-N: MEA employing plain Nafion® membrane (Fig. 1d);
(2) MEA-CeO$_2$: MEA employing CeO$_2$–Nafion membrane (Fig. 1e);
(3) MEA-C (Fig. 1b): MEA with sprayed Nafion® layer with CeO$_2$ nanoparticles facing cathode;
(4) MEA-A (Fig. 1c): MEA with sprayed Nafion® layer with CeO$_2$ nanoparticles facing anode.

The MEAs were fabricated by hot-pressing method at 140 °C and 1 MPa for 1 min. The Pt loadings of the anode and cathode were 0.3 and 0.7 mg cm^{-2}, respectively. Two electrodes with 5 cm^2 effective area were hot-pressed onto a membrane to form a MEA. The MEA was mounted in a single cell using stainless steel as the end plates and stainless steel mesh as the current collectors.

The single cells were run at a cell temperature of 80 °C, 0.2 MPa gas pressure and with externally humidified H$_2$ and O$_2$ both at 80 °C, respectively. After cell performance has been stable for 8 h, the cell voltages at different current densities were recorded.

2.3. Electrochemical impedance spectra (EIS)

In situ electrochemical impedance spectra were measured by employing a KFM2030 impedance meter at 100% RH and 80 °C. The perturbation amplitude for the sinusoidal signal was 165 mA over a frequency range of 10 kHz to 1 Hz. The intercept at high frequencies on the impedance spectra was interpreted as the ohmic resistance of the cell. Area resistances of the cells employing different membranes were measured by EIS.
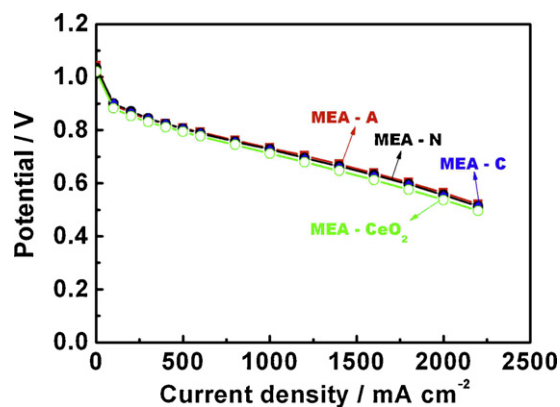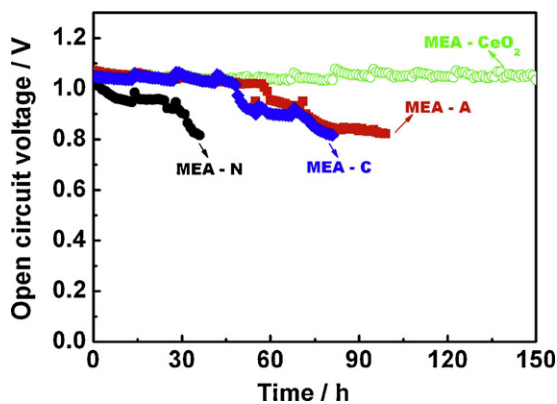

Fig. 6. Durability comparison of different MEAs during OCV tests at 80 °C, 0.2 MPa and 50% RH.
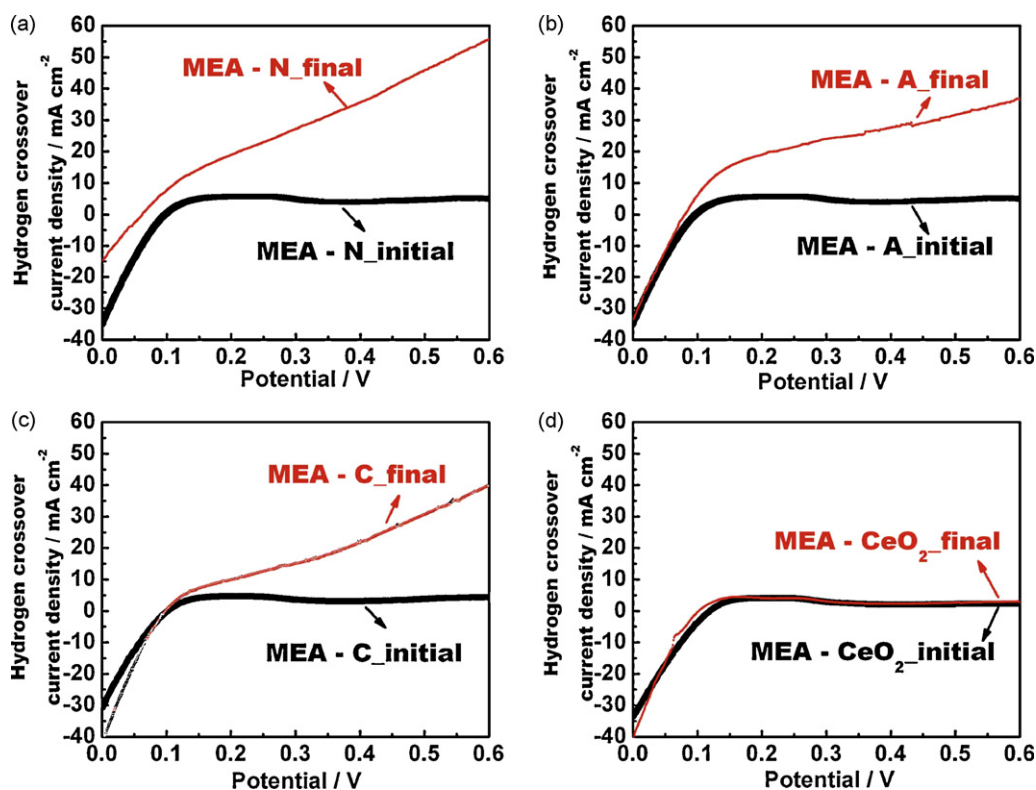
Fig. 7. Hydrogen crossover current density for H_2/N_2 cell with different MEAs before and after OCV tests. H_2 and N_2 gases were humidified at 80 °C and 0.2 MPa.

2.4. XRD measurement of the CeO$_2$ nanoparticles

The X-ray powder diffraction (XRD) analysis on the CeO$_2$ nanoparticles was performed on a PW3040/60 X' Pert PRO (PAN-alytical) diffractometer equipped with a Cu Kα radiation source (λ = 0.15432 nm), operating at 40 kV and 40 mA. A continuous mode was used for collecting data in the 2θ range from 20° to 90°.

2.5. SEM measurement of the novel composite membrane and MEAs

SEM (JEOL 6360LV, Japan) was employed to observe the cross-section morphology of the composite membranes and MEAs before and after OCV tests. The specimens for SEM were prepared by cutting the composite membrane and MEAs with a surgical knife to expose their cross-sections [34].

2.6. Linear sweep voltammetry (LSV) measurement

Hydrogen crossover across the membrane of different MEAs was evaluated by LSV method. Humidified pure hydrogen and nitrogen was fed to the anode and cathode, respectively. The flow rates of H_2/N_2 were controlled at 40 and 100 ml min^{-1}, respectively. The anode, where hydrogen evolution takes place, serves as the counter electrode as well as the dynamic hydrogen reference electrode (DHE). By applying a dynamic potential from 0 to 0.6 V versus the anode with the scan rate of 5 mV s^{-1} at 0.2 MPa, 80 °C and 100% RH, the H_2 oxidation current was measured [31]. The potential was controlled by CHI 600B electrochemical workstation. Hydrogen crossover was evaluated in diffusion-limited hydrogen oxidation current density obtained in the range of 300–350 mV [20].

2.7. In situ membrane durability test

Different MEAs (MEA-N, MEA-A, MEA-C and MEA-CeO$_2$) were tested intermittently under open circuit operation at 80 °C, 0.2 MPa

and 50% RH. H_2 gas was fed to the anode of the cell while O$_2$ was fed to the cathode. The gas flow rate was 40 ml min^{-1}. The OCV of each cell was monitored during the test. The OCV accelerated test was interrupted every 11 h for a stop, and continued on the next day. The open circuit voltages were recorded once per hour after operation conditions were kept sable for about 1 h.

3. Results and discussion

3.1. XRD characterization

XRD was carried out to confirm the structure information of commercial CeO$_2$ nanoparticles (Fig. 2). The commercial CeO$_2$ nanoparticles are crystalline with peaks at 2θ values of 29°, 33°, 48°, 57°, 60°, 70°, 77°, and 79°, which are consistent with previous reports [29,30,35].

3.2. SEM observation of the novel composite membrane

SEM result in Fig. 3 shows the cross-sectional morphology of the novel composite membrane. Two dense layers are clearly observed from the picture; therefore the cross-section of the membrane can be divided into two regions denoted as sections I and II. Section II is 10 μm thick. According to our design, section I is Nafion® 212, and section II is sprayed Nafion® layer with CeO$_2$ nanoparticles.

3.3. Single cell evaluation

Fig. 4 shows the single cell performances of different MEAs (MEA-A, MEA-C, MEA-N, and MEA-CeO$_2$). All the MEAs were evaluated at 80 °C, 0.2 MPa and 100% RH, with oxygen as the oxidant and hydrogen as the fuel. It is observed that the CeO$_2$–Nafion composite membrane exhibits the worst performance due to the increased proton-conductive resistance caused by incorporated non-proton-conductive CeO$_2$ nanoparticles [34]. This is consistent

with the internal resistance evaluated by EIS (Fig. 5). By contrast, the other MEAs (MEA-N, MEA-A and MEA-C) show the similar performance, suggesting that the incorporation of a small quantity of CeO$_2$ nanoparticles on one side of Nafion® 212 does not affect

cell performance. Moreover, the sprayed Nafion® layer was very thin (around 10 μm), and the dispersed CeO$_2$ nanoparticles in the sprayed Nafion® layer did not occupy the whole composite membrane, so the proton conductivity of the section I (Fig. 3) of the
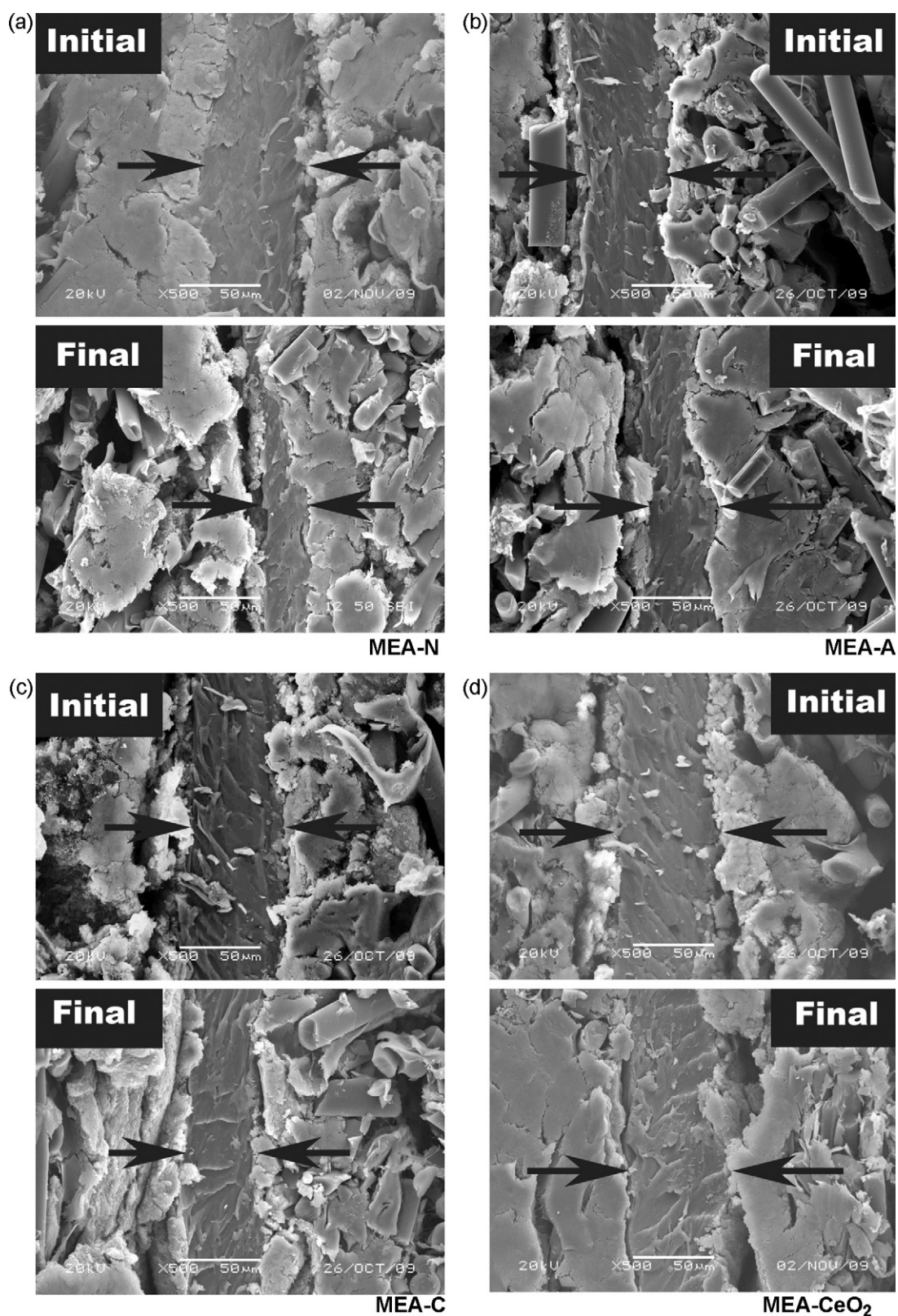

Fig. 8. Comparison of cross-sectional morphology of different MEAs before and after OCV tests. The cathode side is shown left here. (a) MEA-N, (b) MEA-A, (c) MEA-C, and (d) MEA-CeO$_2$.

composite membrane is slightly affected. Therefore, compared with CeO_2–Nafion composite membrane, the other MEAs exhibit little better performance and slightly lower internal resistance (Fig. 5). Overall, the addition of CeO_2 nanoparticles at one side of the membrane does not affect internal resistance, while the CeO_2–Nafion composite membrane with uniformly dispersed CeO_2 nanoparticles increases the internal resistance and lowers performance.

3.4. OCV accelerated test at 50% RH condition

In order to investigate the chemical degradation location of PEMs at open circuit operation, CeO_2 nanoparticles were placed at different locations of the membranes to scavenge free radicals generated there. The radical-initiated membrane degradation is affected by the incorporation of CeO_2 nanoparticles, thus degradation visualization becomes available in terms of OCV decay rate. Fig. 6 shows the results of the OCV accelerated tests of different MEAs (MEA-N, MEA-A, MEA-C and MEA-CeO_2) at 50% RH and 80 °C with H_2/O_2 feed. Among all the MEAs, MEA-N has the shortest lifetime. However, the MEAs incorporated with CeO_2 nanoparticles survive for much longer lifetime than the plain one (MEA-N), irrespective of the locations of CeO_2 nanoparticles (anode, cathode or in the membrane). In the first 45 h, especially, the OCV of MEA-A or C has minor decrease; however, MEA-N degrades dramatically. The different OCV decay rates are ascribed to the embedded CeO_2 nanoparticles, which can scavenge the free radicals generated at anode or cathode [29,30]. But in the last 40 h, MEA-A and MEA-C have similar OCV profiles with MEA-N, suggesting that chemical degradation still takes place in both MEA-A and MEA-C. Because the free radicals, generated at the anode of MEA-A or at the cathode of MEA-C, can be scavenged by CeO_2 nanoparticles embedded there, so the appreciable degradation in the last 40 h of the durability is interpreted as the accumulated radical-initiated membrane degradation at the cathode side of MEA-A and at the anode side of MEA-C. Therefore, it is concluded that the radical-initiated membrane degradation occurs at both sides of anode and cathode at open circuit operation. Moreover, the conclusion is also confirmed by the minor OCV decay rate of MEA-A and MEA-C in the first about 45 h.

In order to further confirm the conclusion, OCV test was carried out on MEA-CeO_2 at the same operation condition as well. MEA-CeO_2 employs the CeO_2–Nafion composite membrane, in which CeO_2 nanoparticles are uniformly dispersed (Fig. 1d). CeO_2 nanoparticles exist at both sides of anode and cathode, which can scavenge free radicals generated at both sides. Therefore, MEA-CeO_2 is supposed to have excellent durability, which is confirmed by the experimental result (Fig. 6). A more stable OCV is obtained by MEA-CeO_2. The OCV decay rate is measured as the ratio of the difference between the initial OCV and the final OCV to the time between the two OCVs [36]. Compared with the OCV decay rate of MEA-N ($5.9\,mV\,h^{-1}$), the OCV decay rates of MEA-X (X = A, C and CeO_2) is 2.5, 2.8, and $0.1\,mV\,h^{-1}$, respectively.

As described above the radical-initiated membrane degradation at open circuit operation takes place at both sides of anode and cathode, which is in accordance with Danilczuk et al.'s report [37].

3.5. Hydrogen crossover measurement

The H_2 permeability of MEAs with different membranes was tested by LSV analysis before and after OCV tests. The representative LSV curves are shown in Fig. 7. The limiting current of each MEA is approximately $5\,mA\,cm^{-2}$ before OCV tests. After OCV tests, no appreciable change in hydrogen crossover of MEA-CeO_2 is observed (Fig. 7d), but considerable changes in hydrogen crossover of the other MEAs are obtained (Fig. 7a–c). That is consistent with the results we get in Fig. 6. The increase in hydrogen crossover indicates

that serious damages such as membrane thinning and micro-hole formation could have occurred during the OCV tests. Although MEA-A and MEA-C have the same trend with MEA-N in hydrogen crossover during the OCV tests, their OCV decay rates are lower than MEA-N, which is ascribed to the suppression of the free radicals by CeO_2 nanoparticles embedded in the sprayed Nafion® layer of the novel composite membrane.

3.6. SEM observation of MEAs before and after OCV test

Cross-sectional SEM images were taken before and after OCV accelerated tests as shown in Fig. 8. In these images the cathode catalyst layer is shown left, and the membrane is located in the middle. From Fig. 8a, the membrane of the MEA-N degrades considerably and becomes thin, so it undergoes the shortest duration at OCV test and the highest OCV decay rate (Fig. 6), which can be related to the large hydrogen crossover current density after OCV test in Fig. 7a. As it is observed from the images of MEA-X (X = A, C and CeO_2) (Fig. 8b–d), the cross-sectional morphology of the membranes after OCV tests are similar to the initial ones, and there are still some extent degradation in terms of the membrane thickness [38,39], the rate of membrane thickness change in MEA-CeO_2 is the lowest of all. That is why the hydrogen crossover current density of MEA-CeO_2 changed much less than the other MEAs after OCV tests (Fig. 7). All these results further confirm that the degradation takes place at both sides of anode and cathode. The focus of the further study is on how the radical-initiated membrane degradation happens, and then more powerful characterizations will be indispensable, such as fluoride emission rate (FER), fourier transform infrared spectroscopy (FTIR).

4. Conclusions

A novel composite membrane using CeO_2 nanoparticles to ascertain the free radical was firstly proposed to investigate the chemical degradation location of proton exchange membrane under open circuit operation. The novel composite membrane is a piece of Nafion® 212 combined with a sprayed Nafion® layer with uniformly dispersed CeO_2 nanoparticles, and the resulting MEAs (MEA-A, MEA-C) with sprayed Nafion® layer facing anode/cathode were subjected to OCV accelerated tests. MEA-A and MEA-C were employed to separate the membrane evaluation process into cathode side and anode side, respectively. Membrane degradation was characterized by OCV decay rate, hydrogen crossover current density and cross-sectional morphology of membrane. It is found that the chemical degradation occurs at both sides of anode and cathode. OCV test was carried out on MEA-CeO_2 at the same operation condition as well to confirm that the chemical degradation takes place at both sides of anode and cathode. This achievement will provide a feasible method to investigate the location of the radical-initiated membrane degradation indirectly.

References

[1] S.M. Haile, D.A. Boysen, C.R.I. Chisholm, R.B. Merle, Nature 410 (2001) 910–913.
[2] B.C.H. Steele, A. Heinzel, Nature 414 (2001) 345–352.
[3] V.O. Mittal, H.R. Kunz, J.M. Fenton, J. Electrochem. Soc. 153 (2006) A1755–A1759.
[4] S.D. Knights, K.M. Colbow, J. St-Pierre, D.P. Wilkinson, J. Power Sources 127 (2004) 127–134.
[5] EG&G Technical Services, Inc., Fuel Cell Handbook, seventh ed., Morgantown, 2004, 88–90.
[6] C. Heitner-Wirguin, J. Membr. Sci. 120 (1996) 1–33.

[7] J.R. Yu, B.L. Yi, D.M. Xing, F.Q. Liu, Z.G. Shao, Y.Z. Fu, Phys. Chem. Chem. Phys. 5 (2003) 611–615.
[8] J. Healy, C. Hayden, T. Xie, K. Olson, R. Waldo, A. Brundage, H. Gasteiger, J. Abbott, Fuel Cells 5 (2005) 302–308.
[9] J.F. Wu, X.Z. Yuan, J.J. Martin, H.J. Wang, J.J. Zhang, J. Shen, S.H. Wu, W. Merida, J. Power Sources 184 (2008) 104–119.
[10] D.E. Curtin, R.D. Lousenberg, T.J. Henry, P.C. Tangeman, M.E. Tisack, J. Power Sources 131 (2004) 41–48.
[11] R. Borup, J. Meyers, B. Pivovar, Y.S. Kim, R. Mukundan, N. Garland, D. Myers, M. Wilson, F. Garzon, D. Wood, P. Zelenay, K. More, K. Stroh, T. Zawodzinski, J. Boncella, J.E. McGrath, M. Inaba, K. Miyatake, M. Hori, K. Ota, Z. Ogumi, S. Miyata, A. Nishikata, Z. Siroma, Y. Uchimoto, K. Yasuda, K.I. Kimijima, N. Iwashita, Chem. Rev. 107 (2007) 3904–3951.
[12] K. Teranishi, K. Kawata, S. Tsushima, S. Hirai, Electrochem. Solid-State Lett. 9 (2006) A475–A477.
[13] S. Zhang, X. Yuan, H. Wang, W. Mida, H. Zhu, J. Shen, S. Wu, J. Zhang, Int. J. Hydrogen Energy 34 (2009) 388–404.
[14] E. Endoh, S. Terazono, H. Widjaja, Y. Takimoto, Electrochem. Solid-State Lett. 7 (2004) A209–A211.
[15] N. Ohguri, A.Y. Nosaka, Y. Nosaka, Electrochem. Solid-State Lett. 12 (2009) B94–B96.
[16] F.D. Coms, ECS Trans. 16 (2008) 235–255.
[17] L. Zhang, S. Mukerjee, J. Electrochem. Soc. 153 (2006) A1062–A1072.
[18] F.A. de Bruijn, V.A.T. Dam, G.J.M. Janssen, Fuel Cells 8 (2008) 3–22.
[19] Z.B. Wang, P.J. Zuo, Y.Y. Chu, Y.Y. Shao, G.P. Yin, Int. J. Hydrogen Energy 34 (2009) 4387–4394.
[20] M. Inaba, T. Kinumoto, M. Kiriake, R. Umebayashi, A. Tasaka, Z. Ogumi, Electrochim. Acta 51 (2006) 5746–5753.
[21] C.D. Huang, K.S. Tan, H.Y. Lin, K.L. Tan, Chem. Phys. Lett. 371 (2003) 80–85.
[22] N. Ramaswamy, N. Hakim, S. Mukerjee, Electrochim. Acta 53 (2008) 3279–3295.
[23] H. Liu, H.A. Gasteiger, A.B. Laconti, J. Zhang, ECS Trans. 1 (2006) 283–293.
[24] M. Aoki, H. Uchida, M. Watanabe, Electrochem. Commun. 8 (2006) 1509–1513.
[25] S. Kundu, M. Fowler, L.C. Simon, R. Abouatallah, J. Power Sources 182 (2008) 254–258.
[26] V. Mittal, H.R. Kunza, J.M. Fentonb, ECS Trans. 1 (2006) 275–282.
[27] F.D. Coms, H. Liu, J.E. Owejan, ECS Trans. 16 (2008) 1735–1747.
[28] S. Babu, A. Velez, K. Wozniak, J. Szydlowska, S. Seal, Chem. Phys. Lett. 442 (2007) 405–408.
[29] P. Trogadas, J. Parrondo, V. Ramani, Electrochem. Solid-State Lett. 11 (2008) B113–B116.
[30] D. Zhao, B.L. Yi, H.M. Zhang, H.M. Yu, L. Wang, Y.W. Ma, D.M. Xing, J. Power Sources 190 (2009) 301–306.
[31] H.L. Tang, M. Pan, S.P. Jiang, X. Wang, Y.Z. Ruan, Electrochim. Acta 52 (2007) 5304–5311.
[32] L. Wang, B.L. Yi, H.M. Zhang, D.M. Xing, Electrochim. Acta 52 (2007) 5479–5483.
[33] L. Ghassemzadeh, M. Marrony, R. Barrera, K.D. Kreuer, J. Maier, K. Müller, J. Power Sources 186 (2009) 334–338.
[34] C. Bi, H.M. Zhang, Y. Zhang, X.B. Zhu, Y.W. Ma, H. Dai, S.H. Xiao, J. Power Sources 184 (2008) 197–203.
[35] M.G. Sujana, K.K. Chattopadyay, S. Anand, Appl. Surf. Sci. 254 (2008) 7405–7409.
[36] V.A. Sethuraman, J.W. Weidner, A.T. Haug, L.V. Protsailo, J. Electrochem. Soc. 155 (2008) B119–B124.
[37] M. Danilczuk, F.D. Coms, S. Schlick, J. Phys. Chem. B 113 (2009) 8031–8042.
[38] M. Aoki, N. Asano, K. Miyatake, H. Uchida, M. Watanabe, J. Electrochem. Soc. 153 (2006) A1154–A1158.
[39] Z.B. Wang, P.J. Zuo, X.P. Wang, J. Lou, B.Q. Yang, G.P. Yin, J. Power Sources 184 (2008) 245–250.